Smart Structures and Systems, *Vol. 35, No. 6 (2025) 315-325*
https://doi.org/10.12989/sss.2025.35.6.315

Guided wave-based cable tension estimation in multi-wire steel strands using principal component analysis

Ru Zhang [1,2,3a], Xiaodong Sui*[1,2,3], Yuanfeng Duan [2b] and Yaozhi Luo [2c]

[1] *Department of Civil Engineering, Hangzhou City University, China*
[2] *College of Civil Engineering and Architecture, Zhejiang University, China*
[3] *Zhejiang Key Laboratory of Safe Construction and Intelligent Maintenance for Urban Shield Tunnels, China*

(*Received June 10, 2025, Revised June 23, 2025, Accepted June 26, 2025*)

Abstract. In-service monitoring of the stress state of steel strands or cables is essential for estimating the loading capacity of the entire structure. The traditional wave velocity–based method may not be sensitive to changes in cable tension. To address this issue, a principal component analysis (PCA)-based method was presented in this study, using longitudinal guided waves generated by a pair of magnetostrictive transducers. First, semi-analytical finite element analysis was performed considering the effect of the external load to investigate the changes in wave velocity under various guided wave modes in the lower frequency range. Then, experimental studies were conducted on a seven-wire steel strand under various cable tension levels. The direct-arrival wave packets of the reference signals were used to construct the PCA model. Score values corresponding to the principal components (PCs) of the reference signals were calculated, and the PCs whose scores were closely related to the tension variations were determined. A linear regression curve for the scores and cable tensions was constructed and used to determine the cable tensions for the test signals. The results show that the proposed method can accurately estimate cable tension and performs better than the notch frequency-based method.

Keywords: cable tension estimation; guided wave; magnetostrictive transducers; principal component analysis; Q-statistics; scores; steel strands

1. Introduction

Multiple-wire steel strands are widely used in numerous industries. They are integral parts of various structures, including cable-supported bridges and elevators, providing essential support and stability to ensure the safety of the structure (Rizzo and Di Scalea 2006). There is a considerable demand for cable force (tension) measurements during both the construction and operation stages (Jo *et al*. 2021, Jana *et al*. 2022). During construction, precise control of the cable force can prevent excessive structural deformation and stress concentration, thereby ensuring the safety and quality of construction works. In the operation phase, cables are subjected to various stresses, such as fatigue load and local damage, which may lead to the degradation of their load-bearing capacity. Therefore, effective methods for in situ evaluation of cable tension must be developed (Piciucco *et al*. 2024).

Vibration-based method has been commonly used to estimate cable tension in air (Zui *et al*. 1996, Cho *et al*. 2010). In this method, cable tensions are determined using the relationship between the tension and vibration frequencies, which is commonly estimated from the acceleration responses. The estimation errors of this method generally lied in the range of 5%–10% (Zarbaf *et al*. 2018). However, the dynamic properties of cables are influenced by boundary conditions, particularly for short cables (Kong *et al*. 2024). Recently, vibration-based methods for the real-time estimation of cable tension have been studied using wireless sensors and computer-vision techniques (Cho *et al*. 2010, Wangchuk *et al*. 2022, Shang *et al*. 2024). Several nondestructive testing methods have been introduced to estimate the cable tension, including the fiber optic sensor method, electromagnetic-based method, and guided wave method (Yim *et al*. 2013, Yao *et al*. 2021, Ng *et al*. 2022, Wang *et al*. 2022). Fiber optic sensors need be either attached to the outer surface or embedded into the cable during construction to measure strain changes (Sahota *et al*. 2020), limiting their applicability primarily to newly constructed structures. The electromagnetic method capitalizes on the magneto-elastic effect of ferromagnetic materials, where the magnetic properties of steel cables alter under varying external tensions (Wang *et al*. 2006, Ren *et al*. 2018, Park *et al*. 2022, Zhang *et al*. 2022). The elasto-magnetic (EM) sensor generally comprises a primary coil for magnetization and a secondary coil for actuation and sensing. To improve the tension estimation accuracy, Duan *et al*. (2016) introduced an elasto-magneto-elastic (EME) sensor by substituting the secondary coil with a smart magneto-electric unit, and developed temperature compensation algorithms (Zhang *et al*. 2018b). Kim *et al*.

*Corresponding author, Ph.D., Post Doctor,
E-mail: xdsui@zju.edu.cn
[a] Professor, E-mail: zhangru@hzcu.edu.cn
[b] Professor, E-mail: ceyfduan@zju.edu.cn
[c] Professor, E-mail: luoyz@zju.edu.cn

ISSN: 1738-1584 (Print), 1738-1991 (Online)

(2010) proposed a unique guided wave method for cable tension estimation, which is particularly advantageous for steel strands grouted within concrete and in the anchorage zones.

The existing guided wave–based methods for estimating cable tension mainly include wave velocity–based, notch frequency–based, and attenuation characteristics–based methods. Chaki and Bourse (2009) presented a simplified acoustoelastic model for seven-wire steel strands and verified it using the first-order longitudinal mode (L(0, 1)) generated by magnetostrictive (MS) transducers. The phase changes in the received signals at various cable tensions were extracted to assess the variations in wave velocity, which were found to be quite small. Kwun *et al*. (1998) observed the notch frequency phenomenon during the application of axial stress to a steel strand, noting that certain frequency components disappeared on the received signal from the spectrum, with the central frequency of the missing range increasing with cable tension. Two frequency peaks appeared on two sides of the notch frequency, with the central frequency of the right peak employed as the cable tension estimation index. Liu *et al*. (2017) conducted experimental tests to study the sensitivity of the notch frequency to low-intensity cable tension. The notch frequency was found to be caused by the contact forces between adjacent wires (Bartoli *et al*. 2012). However, there are currently no theoretical explanations for the notch frequency. The contact forces between wires will also affect the attenuation properties of the guided waves. In this light, Chen *et al*. (2022) proposed an energy propagation model for cables that considers the wave energy transmission among wires. The experimental results indicated that cable tension can affect the received wave energy, but the stability of this method requires further investigation.

The dispersion properties of seven-wire steel strands under an external load should be well understood to select the appropriate parameters of the excitation signal. As the Pochhammer–Chree equation is not applicable to multi-wire structures, several alternative methods have been proposed, including the semi-analytical finite element (SAFE) method, scaled boundary finite element (FE) method, and waveguide FE method (Gravenkamp *et al*. 2013, Schaal *et al*. 2013, Zhang *et al*. 2018a). Zhang *et al*. (2018a) investigated the effect of the number of wires on the dispersion properties, reporting that the cutoff frequency for the higher modes decreases with increasing number of wires. This suggests that the lower-frequency range is appropriate for selecting the excitation frequency. Treyssede (2008) introduced a helical coordinate system into the SAFE model to calculate dispersion curves for strands with helical wires. Tang *et al*. (2021) compared the group velocity dispersion curves for a steel strand with seven helical wires in Cartesian and helical coordinate systems. Two results for the L(0, 1) mode are very similar, but computational efficiency is higher when using the Cartesian coordinate system. To the best of the author's knowledge, the effects of axial loads on the wave velocities in each guided wave mode have not been elucidated. Thus, herein, they were investigated using the SAFE model.

Principal component analysis (PCA) is a classic multivariate statistical analysis method that is widely used in fields such as data dimensionality reduction, feature extraction, and damage detection (Park *et al*. 2007, Mujica *et al*. 2011, Tu *et al*. 2021). PCA projects the original data onto a new coordinate system consisting of principal components (PCs) through a linear transformation. Each PC may be closely related to physical features, such as temperature changes, exciting frequencies, local damage, and cable tension. Therefore, effective information about a certain feature can be extracted from PC scores, whereas unwanted signal components can be removed. The T^2 and Q indices are often used to analyze the variability of the projected data in the selected principal subspace and outliers from the subspace, respectively, thereby quantifying the differences between the reference and test data (Mujica *et al*. 2011).

In this study, a SAFE model that accounts for cable tension was constructed to analyze changes in wave velocity for various modes and provide the basis for selecting appropriate excitation signals. Considering the shortcomings of the wave velocity–based and notch frequency–based methods in terms of feasibility in practical applications and tension estimation accuracy, a novel PCA-based method was proposed using L(0, 1) guided wave signals obtained from a pair of MS transducers. In this method, score values most sensitive to tension variations are used as the tension estimation indices. The remainder of this paper is organized as follows: In Section 2, dispersion analysis of a seven-wire steel strand including the cable tension effect was presented. In Section 3, the structure of the MS transducer for generating the L(0, 1) wave and the PCA-based cable tension estimation method were introduced. Experimental tests on the proposed method were performed, with the results shown in Section 4. Section 5 gives the brief conclusions.

2. Dispersion analysis of the steel strand

2.1 SAFE method

The SAFE method allows the highly computationally efficient analysis of the dispersion properties of a waveguide with an arbitrary cross-section. Its efficiency stems from the assumption that a wave propagates along the longitudinal direction in a harmonic exponential solution. A detailed theory of the SAFE method can be found in the author's previous research (Tang *et al*. 2021). The seven-wire steel strand employed in this study comprises six helical wires surrounding one straight wire as in Fig. 1. The material and geometrical properties of the steel strand are listed in Table 1. In the absence of external tension, the strain–kinetic energy relationship can be expressed as

$$\int_{\Omega}\delta\boldsymbol{\varepsilon}^{\mathrm{T}}\boldsymbol{\sigma}dxdydz-\omega^{2}\int_{\Omega}\rho\delta\mathbf{u}^{\mathrm{T}}\mathbf{u}dxdydz=0 \qquad (1)$$

where, $\mathbf{u}$ is the displacement vector; $\boldsymbol{\sigma}$ and $\boldsymbol{\varepsilon}$ are the stress and strain vectors, respectively; ω is the angular frequency; ρ is the density; and Ω is the element volume. Eq. (2) can be derived from Eq. (1) as (Zhang *et al*. 2018a)

(a) Phase velocity (b) Group velocity

Fig. 1 Dispersion curves of the steel strand: no axial tension

Table 1 Material and geometrical parameters of the seven-wire steel strand

Young's modulus (GPa)	Density (kg/m^3)	Poisson ratio	Wire diameter (mm)	Outer diameter (mm)	Peripheral pitch (mm)
210	7850	0.28	5.1	15.2	260

$$(\boldsymbol{K_1} + ik\boldsymbol{K_2} + k^2\boldsymbol{K_3} - \omega^2\boldsymbol{M})\boldsymbol{U} = 0 \tag{2}$$

where, $\boldsymbol{U}$ is the global displacement matrix; $\boldsymbol{K_1}$, $\boldsymbol{K_2}$, and $\boldsymbol{K_3}$ are the global stiffness matrices; and $\boldsymbol{M}$ is the global mass matrix. Dispersion curves of the phase velocity and group velocity can be obtained by solving Eq. (2), as shown in Fig. 1. The curves for the longitudinal (L(0, 1)), torsional (T(0, 1)), and flexural (F(1, 1)) modes exhibit smooth behavior in the lower frequency range, whereas the dispersion properties become complex when the excitation frequency exceeds 100 kHz.

2.2 Changes in wave velocity under axial stress

According to acoustoelastic theory, the longitudinal (C_L^σ) and transverse (C_T^σ) wave velocities of a slender homogeneous and isotropic waveguide under axial stress in the z-direction can be expressed as (Chaki and Bourse 2009)

$$\begin{aligned} C_L^\sigma &= \sqrt{\frac{\lambda+2\mu}{\rho}}\left\{1+\frac{\sigma_{zz,0}}{2(\lambda+2\mu)(3\lambda+2\mu)}\times\left(\frac{\lambda+\mu}{\mu}(4\lambda+10\mu+4m)+\lambda+2l\right)\right\} \\ C_T^\sigma &= \sqrt{\frac{\mu}{\rho}}\left\{1+\frac{\sigma_{zz,0}}{2\mu(3\lambda+2\mu)}\times\left(4\lambda+4\mu+m+\frac{\lambda n}{4\mu}\right)\right\} \end{aligned} \tag{3}$$

where, $\sigma_{zz,0}$ is the initial axial stress; λ and μ are the Lamé elastic constants; and m, n, and l are the Murnaghan third-order elastic constants. It has been found that both C_L^σ and C_T^σ decrease under the axial stress. The changes in the elastic constants ($\lambda, \mu, m, n, and\ l$) are found to be very small (Chaki and Bourse 2009), resulting in the minor variations in wave velocities.

The wave propagation properties of the guided waves under axial loads were analyzed by SAFE model in this study. The linear strain–displacement relationship was typically employed, and higher-order strain components were neglected when analyzing cases without axial stress. This is because the amplitude of the strain induced during wave propagation is similar to that of the excitation signal. However, the amplitude of the guided wave is much smaller than the initial strain caused by the axial load. Thus, higher-order strain components should be included, and the strain $\boldsymbol{\varepsilon}$ in Eq. (1) is expressed as

$$\boldsymbol{\varepsilon} = \begin{Bmatrix} \frac{\partial u_x}{\partial x}+\frac{1}{2}\left[\left(\frac{\partial u_x}{\partial x}\right)^2+\left(\frac{\partial u_y}{\partial x}\right)^2+\left(\frac{\partial u_z}{\partial x}\right)^2\right] \\ \frac{\partial u_y}{\partial y}+\frac{1}{2}\left[\left(\frac{\partial u_x}{\partial y}\right)^2+\left(\frac{\partial u_y}{\partial y}\right)^2+\left(\frac{\partial u_z}{\partial y}\right)^2\right] \\ \frac{\partial u_z}{\partial z}+\frac{1}{2}\left[\left(\frac{\partial u_x}{\partial z}\right)^2+\left(\frac{\partial u_y}{\partial z}\right)^2+\left(\frac{\partial u_z}{\partial z}\right)^2\right] \\ \frac{\partial u_x}{\partial y}+\frac{\partial u_z}{\partial x}+\frac{\partial u_x}{\partial x}\cdot\frac{\partial u_x}{\partial y}+\frac{\partial u_y}{\partial x}\cdot\frac{\partial u_y}{\partial y}+\frac{\partial u_z}{\partial x}\cdot\frac{\partial u_z}{\partial y} \\ \frac{\partial u_y}{\partial z}+\frac{\partial u_z}{\partial y}+\frac{\partial u_x}{\partial y}\cdot\frac{\partial u_x}{\partial z}+\frac{\partial u_y}{\partial y}\cdot\frac{\partial u_y}{\partial z}+\frac{\partial u_z}{\partial y}\cdot\frac{\partial u_z}{\partial z} \\ \frac{\partial u_x}{\partial z}+\frac{\partial u_z}{\partial x}+\frac{\partial u_x}{\partial x}\cdot\frac{\partial u_x}{\partial z}+\frac{\partial u_y}{\partial x}\cdot\frac{\partial u_y}{\partial z}+\frac{\partial u_z}{\partial x}\cdot\frac{\partial u_z}{\partial z} \end{Bmatrix} \tag{4}$$

The element strain energy ($\Phi_{(e)}$) in Eq. (1) under the initial axial stress $\boldsymbol{\sigma}_{zz,0}$ becomes

$$\begin{aligned} \Phi_{(e)} = &\frac{1}{2}\boldsymbol{\sigma}_{(e)}^T\cdot\boldsymbol{\varepsilon}_{(e)}+\boldsymbol{\sigma}_{zz,0}\cdot\frac{\partial u_z}{\partial z} \\ &+\boldsymbol{\sigma}_{zz,0}\cdot\frac{1}{2}\left[\left(\frac{\partial u_x}{\partial z}\right)^2+\left(\frac{\partial u_y}{\partial z}\right)^2+\left(\frac{\partial u_z}{\partial z}\right)^2\right] \end{aligned} \tag{5}$$

Then, Eq. (2) is rewritten as

$$\begin{aligned} &\left(\boldsymbol{K_1}+ik\boldsymbol{K_2}+k^2(\boldsymbol{K_3}+\boldsymbol{K}^{(\sigma)})-\omega^2\boldsymbol{M}\right)\boldsymbol{U}=0 \\ &\boldsymbol{K}^{(\sigma)}=\frac{\sigma_{zz,0}}{\rho}\boldsymbol{M} \end{aligned} \tag{6}$$

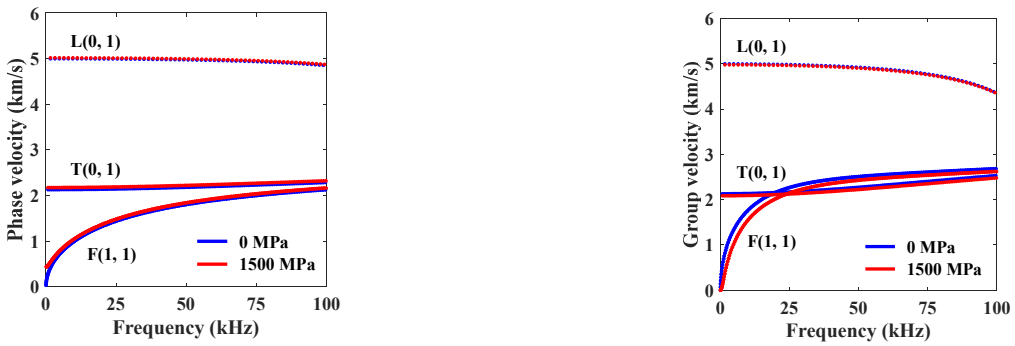

(a) Phase velocity (b) Group velocity

Fig. 2 Dispersion curves under the tensile stress of 1500 MPa

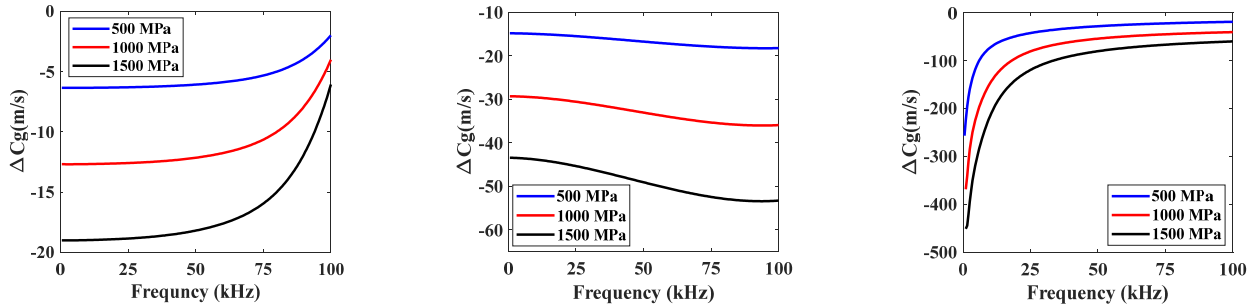

(a) L(0, 1) (b) T(0, 1) (c) F(1, 1)

Fig. 3 Group velocity changes of each mode under different tensile stresses

The ultimate tensile strength of the seven-wire steel strand is 1860 MPa. The phase and group velocity dispersion curves under a tensile stress of 1500 MPa are shown in Fig. 2. It can be found that the wave velocity slightly decreases, which agrees with the acoustoelastic theory in Eq. (3). The wave velocity change is distinct in the lower-frequency range and minimal in the higher-frequency range. This agrees with the results obtained by Chen and Wilcox (2007) using FE simulations. Fig. 3 illustrates the changes in group velocity (ΔC_g) for each mode under various tensile stresses relative to the velocities without external stress. Notably, F(1, 1) exhibits a relatively larger group velocity change than L(0, 1) and T(0, 1). However, the generation of pure torsional and flexural waves in multi-wire structures still remains a considerable challenge. Thus, the L(0, 1) mode, generated by an MS transducer, was used in this study. The test equipment used in this study works well in the lower-frequency range. The central frequency of the MS transducer was designed as 80 kHz, where the signal amplitude reaches its maximum. Thus, the excitation frequency was taken as 80 kHz. The maximum ΔC_g is only 0.3% at 1500 MPa, which is hard to detect in practice because of various uncertainties.

3. Theory of guided wave–based cable tension estimation

3.1 Structure of MS transducers

Piezoelectric and MS transducers are commonly used to generate longitudinal guided waves. The piezoelectric transducer has to be attached to the cross-section of the cable, which may not be feasible for cables with a polyethylene sheath or inaccessible ends. The MS transducers take advantages of its non-contact and moveable nature. The MS transducers used in this study consist of three sets of magnetizers to provide the static magnetic field and a coil unit to provide the dynamic magnetic field, as shown in Fig. 4. Each magnetizer consists of two permanent magnets and a yoke. The static and dynamic magnetic fields are parallel to the axial direction of the seven-wire steel strand to generate longitudinal guided waves. The detailed design and parameter optimization of MS transducers based on multiphysics FE simulations can be found in our previous study (Sui *et al*. 2025).

The MS coefficient of the transducer is also affected by the cable tension. According to the Jiles–Ather–Sablik model (Xu *et al*. 2019), the effective static magnetic field intensity (H_e) in the steel strand is given by

$$H_e = H + \alpha M + H_\sigma$$
$$H_\sigma = \frac{3}{2}\left(\frac{\sigma}{\gamma M_s}\right)\left\{\frac{M}{M_s}\left[\eta_1 + \frac{3}{2}\eta_3\left(\frac{M}{M_s}\right)^3\right]\right\} \quad (7)$$

where, H is the magnetic field intensity provided by the permanent magnets; α is the mean field parameter; M is the magnetization intensity; M_s is the saturation magnetization intensity; H_σ is the effective magnetic field intensity induced by the cable tension; γ is the magnetic permeability in air; and η_1 and η_3 are the coefficients related to the material. When the steel strand is subjected to an external

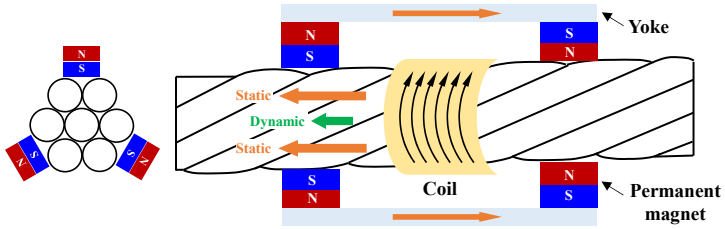

Fig. 4 Structure and magnetic field distribution of the MS transducer

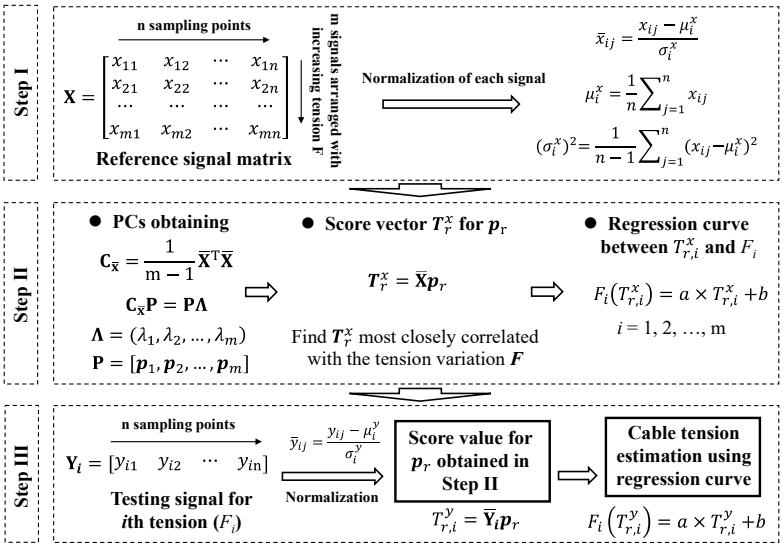

Fig. 5 Flowchart of the PCA-based cable tension estimation method

tension, the static magnetic field increases, thereby changing the MS coefficient of the MS transducer. As a result, the amplitude and phase of the received signal changes depending on cable tension.

3.2 PCA-based cable tension estimation using score values

PCA was used to distinguish minor differences in the guided wave signals resulting from different cable tensions. This was achieved by constructing a new coordinate space in which variance is maximized and the correlation among variables is minimized. In this study, the PCA-based cable tension estimation was carried out by following the three steps shown in Fig. 5.

Step I. Reference data collection and normalization: A pair of MS transducers arranged in a pitch–catch configuration was used to obtain longitudinal guided wave signals. A set of m experiments was conducted on the seven-wire steel strand at various cable tension levels. The received signals consisting of n sampling points were selected to construct a reference signal matrix $\mathbf{X}$. Subsequently, the signals were normalized using Eq. (8).

$$\bar{x}_{ij} = \frac{x_{ij} - \mu_i^x}{\sigma_i^x}; \qquad \mu_i^x = \frac{1}{n}\sum_{j=1}^{n} x_{ij}$$
$$(\sigma_i^x)^2 = \frac{1}{n-1}\sum_{j=1}^{n}(x_{ij} - \mu_i^x)^2 \tag{8}$$

Step II. PC extraction: The normalized reference signal matrix ($\bar{\mathbf{X}}$) was used to construct the covariance matrix ($\mathbf{C}_{\bar{\mathbf{x}}}$) as follows

$$\mathbf{C}_{\bar{\mathbf{x}}} = \frac{1}{\mathrm{m}-1}\bar{\mathbf{X}}^{\mathrm{T}}\bar{\mathbf{X}} \tag{9}$$

Singular value decomposition was applied to $\mathbf{C}_{\bar{\mathbf{x}}}$, yielding m eigenvalues and m eigenvectors, which are the PCs ($\boldsymbol{p}_i$, i = 1, 2, …, m). The score value ($\boldsymbol{T}_r^x$) for the rth PC ($\boldsymbol{p}_r$) can be calculated as follows

$$\boldsymbol{T}_r^x = \bar{\mathbf{X}}\boldsymbol{p}_r \tag{10}$$

After finding $\boldsymbol{T}_r^x$ that is closely correlated with the tension variation $\boldsymbol{F}$ in the m reference signals, a regression curve between $T_{r,i}^x$ and the applied cable tension F_i was established as

$$F_i\left(T_{r,i}^x\right) = a \times T_{r,i}^x + b \tag{11}$$

where $T_{r,i}^x$ and F_i are the score and tension for the ith reference signal, respectively; and a and b are linear regression coefficients.

Step III. Cable tension estimation for the test case: The testing signal vector ($\mathbf{Y}_i$) was obtained with n data points.

The same data processing method as in Step I was used to obtain the normalized signal vector ($\bar{\mathbf{Y}}_i$), and the score value ($T_{r,i}^y$) for the rth PC was calculated as

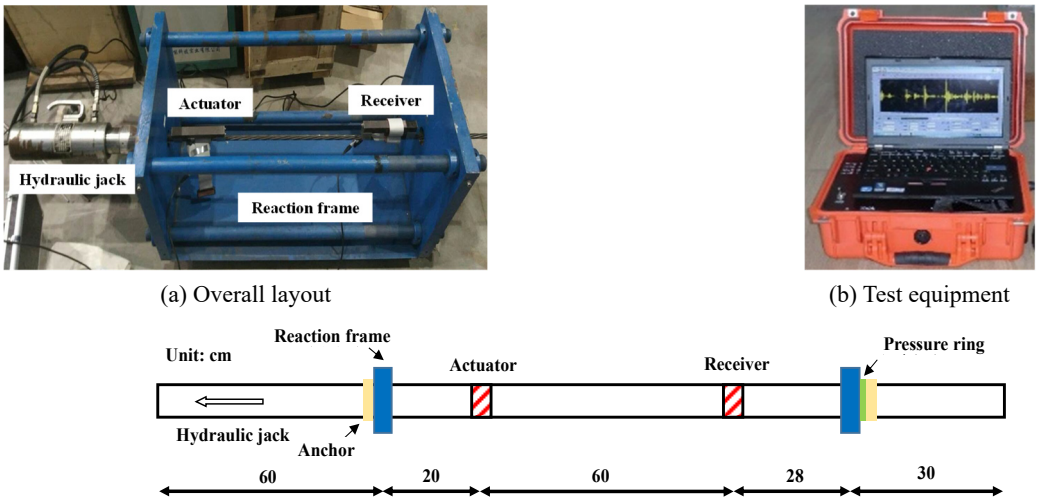

(a) Overall layout (b) Test equipment

(c) Distribution of the transducers

Fig. 6 Experimental setup

$$T_{r,i}^{y} = \bar{\mathbf{Y}}_i \boldsymbol{p}_r \tag{12}$$

Finally, the cable tension $F_i(T_{r,i}^{y})$ for the test case was determined from the regression curve (Eq. (11)).

4. Experimental study

4.1 Experimental setup

Experiments were carried out to verify the proposed PCA-based method for estimating cable tension on a seven-wire strand with the same material and geometrical properties as in Table 1. The total length of the steel strand was 1.98 m. The experimental setup is shown in Fig. 6(a). A reaction frame was designed to apply the cable tension. The steel strand passed through the holes on both sides of the reaction frame. The right side was fixed to the anchor head with clips, while the left side was connected to the hydraulic jack, which was controlled by an oil pump to apply axial load. A pressure ring connected to an electronic pressure gauge was placed between the right anchor and the reaction frame to measure cable tension in real time. Two MS transducers were installed on the steel strand at a distance of 0.6 m, as shown in Fig. 6(c). The parameters of the employed MS transducers are the same as those in the reference (Sui *et al*. 2025). The distance should not be set too short to prevent the masking of the direct-arrival wave packet by the crosstalk signal of the equipment. The left transducer functioned as an actuator, and the right one served as a receiver. The excitation, reception, signal synchronization, and preliminary processing of the guided waves were accomplished using the testing equipment developed by Hangzhou Zheda Jingyi Electromechanical Technology Co., LTD as shown in Fig. 6(b), which was wirelessly connected to the laptop. The excitation signal was a five-cycle sinusoidal tone burst with a frequency of 80 kHz as shown in Fig. 7. The excitation signal was amplified by the test equipment before being input into the coil, with the maximum driving voltage reaching 270 V. For each measurement, the signal was excited 20 times. The received signals were also amplified and modulated, with the averaged signal sent to the laptop. The sampling frequency was set to 1 MHz. The tests were conducted in an indoor environment with a nearly constant ambient temperature.

4.2 Wave velocities at various levels of cable tension

An example of the received signals at 50 kN is shown in Fig. 8. The first wave packet is the unavoidable crosstalk signal, and the second wave packet is the direct-arrival longitudinal guided wave. Since there is a bandwidth in the excitation signal, weak dispersion existed during the wave propagation process, resulting in the number of cycles in the direct-arrival wave packet being larger than that of the

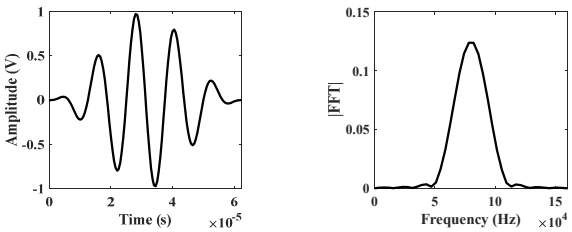

(a) Time domain (b) Frequency domain

Fig. 7 Five-cycled tone burst excitation signal with 80 kHz

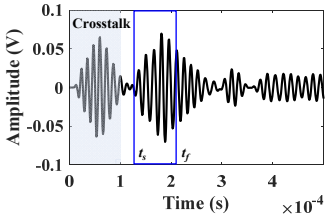

Fig. 8 Received signal under 50 kN

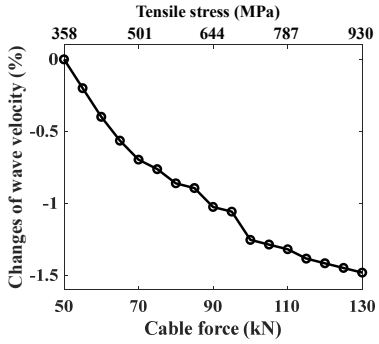

Fig. 9 Changes of the wave velocity under various cable tensions

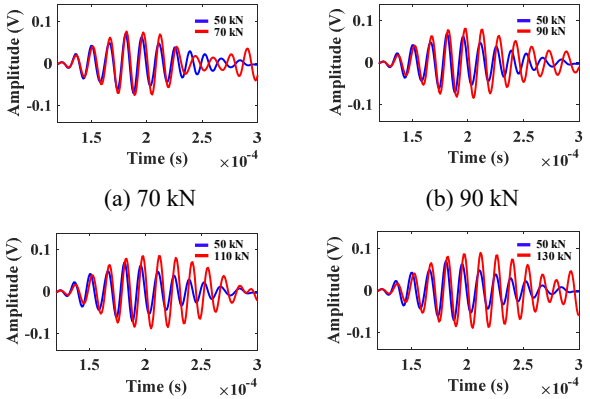

(a) 70 kN (b) 90 kN

(c) 110 kN (d) 130 kN

Fig. 10 Direct incoming wave under various tensions

excitation signal (5). In addition, oscillations in the MS transducer may have also affected the received signal. The wave velocity was obtained as 4959 m/s based on the distance between the actuator and the receiver (0.6 m) and the time of flight of the direct-arrival wave packet (121 μs). The wave velocity of the L(0, 1) mode at 80 kHz was obtained as 4864 m/s from the SAFE model, which agrees well with the experimental result with a relative error of less than 2%. Fig. 9 shows the changes in wave velocity at various cable tension levels from 50 to 130 kN. The wave velocity gradually decreases with increasing cable tension. The maximum wave velocity change is only 1.5%, which may not be detected in practical applications. The measured velocity variation (1.5%) is found to be slightly larger than the SAFE analysis result (0.3%). The received signals at 70, 90, 110, and 130 kN are shown in Fig. 10. Both the phase and amplitude changed with the cable tensions.

4.3 Cable tension estimation using score values

The loading range of the cable tension was from 50 to 130 kN, with an interval of 5 kN. The direct incoming waves at 50, 60, 70, 80, 90, 100, 110, 120, and 130 kN were utilized to construct the reference signal matrix, whereas the signals at other cable tension levels were used to test the performance of the proposed method. The experiment was repeated 15 times for each cable tension level. Guided wave

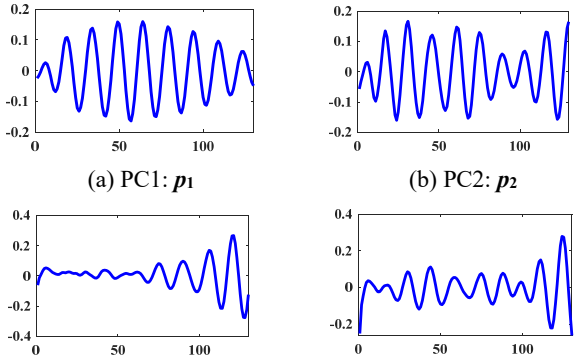

(a) PC1: $\boldsymbol{p}_1$ (b) PC2: $\boldsymbol{p}_2$

(c) PC3: $\boldsymbol{p}_3$ (d) PC4: $\boldsymbol{p}_4$

Fig. 11 First four PCs (Δt = 1 μs)

Table 2 First six eigenvalues and their contribution weights (t_f= 250 μs)

PCs	1	2	3	4	5	6
Eigenvalues	6.926	0.319	0.092	0.011	0.003	0.001
Contribution weights (%)	94.19	4.34	1.25	0.15	0.04	0.01

signals during time period [t_s, t_f] were extracted with Δt of 1 μs to form the reference signal matrix. Here, t_s is the instant when the longitudinal guided wave arrives at the receiver, which equals 121 μs. The value of t_f was set to 250 μs, while 2 other values of t_f will be considered for comparison at the end of the current section. The reference signals were arranged in the order of increasing cable tension. The size of the reference signal matrix $\mathbf{X}$ in Fig. 5 is 135 × 130. After the normalization of $\mathbf{X}$ into $\bar{\mathbf{X}}$, singular value decomposition was conducted on the covariance matrix $\mathbf{C}_{\bar{\mathbf{X}}}$ to obtain the eigenvectors, which are the PCs. The first six eigenvalues are listed along with their contribution weights to the sum of all eigenvalues in Table 2. The contribution weights of the first and second PCs are 94.19% and 4.34%, respectively, while those of the rest of the PCs are relatively small. Fig. 11 shows the first four PCs.

The score values for the 135 reference signals corresponding to the first four PCs are shown in Fig. 12. The trends in the score values for $\boldsymbol{p}_1$ and $\boldsymbol{p}_2$ are closely related to the variation in cable tension. The score values for $\boldsymbol{p}_3$ decrease with the increasing tension till 90 kN. Then they begin to increase afterwords. The relationship between the score and cable tension becomes more complex for $\boldsymbol{p}_4$. For $\boldsymbol{p}_1$, a second-order regression curve was obtained as $y = -0.0003x^2 + 0.075x - 1.135$ ($R^2 = 0.881$), where x is the cable tension and y is the score value for the PC. On the other hand, a linear relationship was obtained for $\boldsymbol{p}_2$ as $y = -0.021x + 1.968$ ($R^2 = 0.950$), as shown in Fig. 13. However, the relationship between the score for $\boldsymbol{p}_3$ and the cable tension is not monotonic. Variations in scores for $\boldsymbol{p}_1$ are small at large cable tension levels. Therefore, the linear regression curve obtained from $\boldsymbol{p}_2$ was used to estimate the cable tension. The estimation accuracy was then examined for test cases with cable tensions of 55, 65, 75, 85, 95, 105, 115, and 125 kN, as listed in Table 3. The maximum

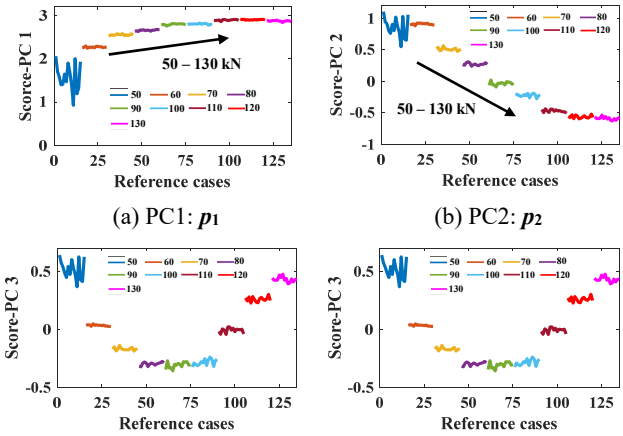

(a) PC1: $\boldsymbol{p}_1$ (b) PC2: $\boldsymbol{p}_2$

(c) PC3: $\boldsymbol{p}_3$ (d) PC4: $\boldsymbol{p}_4$

Fig. 12 Scores of the reference signals corresponding to the first four PCs

Table 3 Estimated cable tensions (t_f = 250 μs)

Real tensions (kN)	Scores (Average and COV* (%))	Estimated cable tension (kN) (Average and COV* (%))	Average error (%)
55	0.861 (2.41)	52.48 (2.72)	4.58
65	0.637 (3.71)	63.09 (1.99)	2.94
75	0.396 (5.96)	74.51 (1.50)	0.66
85	0.109 (25.29)	88.11 (1.49)	3.66
95	-0.132 (13.68)	99.54 (1.13)	4.78
105	-0.356 (7.85)	110.18 (1.20)	4.93
115	-0.529 (3.55)	118.37 (0.75)	2.93
125	-0.577 (6.68)	120.63 (1.51)	3.50

*COV in parentheses are the coefficient variation.

estimation error is 4.93%, indicating the excellent performance of the proposed method.

The length of the signal in the reference signal matrix was also discussed for two other t_f values, 183 and 300 μs. In the case of 183 μs, the interval between t_f and t_s equals the duration of the excitation signal. The results are shown in Fig. 14. The regression curves were obtained as $y = -0.012x + 1.130$ ($R^2 = 0.967$) for t_f of 183 μs, and $y = -0.026x + 2.402$ ($R^2 = 0.896$) for t_f of 300 μs. The estimated cable tension values for the tested cases are listed in Table 4. The maximum errors are 4.56% and 12.06% for t_f of 183 and 300 μs, respectively. Overall, the errors for cases with t_f

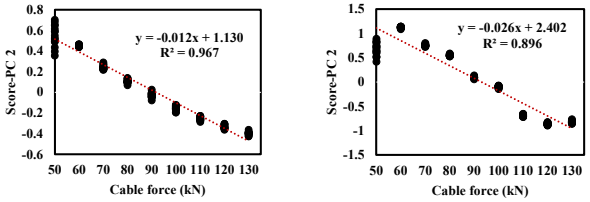

(a) t_f = 183 μs (b) t_f = 300 μs

Fig. 14 Relationship between scores and cable tensions for different signal lengths

Table 4 Estimated cable tensions using two different signal lengths

Real tensions (kN)	t_f = 183 μs		t_f = 300 μs	
	Average estimates (kN)	Average errors (%)	Average estimates (kN)	Average errors (%)
55	54.29	1.29	53.95	1.91
65	63.93	1.65	57.16	12.06
75	77.65	3.54	66.73	11.02
85	88.87	4.56	80.63	5.14
95	98.77	3.97	99.51	4.74
105	108.38	3.22	108.44	3.28
115	115.67	0.58	124.87	8.58
125	121.76	2.59	125.92	0.74

of 183 μs are smaller than the other cases. Thus, t_f was adopted as 183 μs.

4.4 Cable tension estimation using Q-statistics

The performance of the proposed score-based method was compared with that of the Q-statistics method, in which the reference signal matrix is constructed from a single cable tension level. In this case, 40 sets of received signals at 50 kN were used as the reference signals, while signals obtained from 55 to 130 kN were used to form the normalized testing signal matrix $\overline{\mathbf{Y}}$. The first four PCs were selected to calculate the Q-statistic as follows

$$\mathrm{Q} = \overline{\mathbf{Y}}(\mathbf{I} - \mathbf{P}_{n\times 4}\mathbf{P}_{n\times 4}^{\mathrm{T}})\overline{\mathbf{Y}}^{\mathrm{T}} \tag{13}$$

The cumulative weight of the first four PCs is 99.81%. The Q-statistic represents unusual variation (in cable tension in the present case) out of the principal subspace

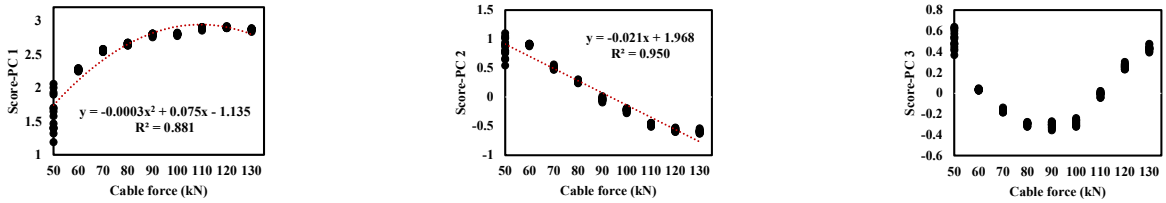

(a) PC1 (b) PC2 (c) PC3

Fig. 13 Relationship between scores and cable tensions of the reference signals

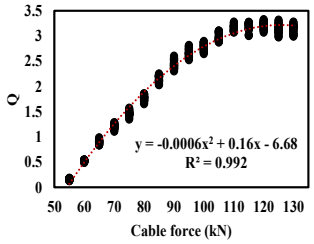

Fig. 15 Relationship between the Q-statistics of testing signals and cable tensions

spanned by the selected PCs. The Q-statistics method is easier to implement, because it requires reference signals from only a single tension level whereas the score-based method necessitates data from various tension levels. Collecting signals at multiple tension levels can be challenging in practical applications. Therefore, the reference signals for the score-based method may be obtained using cable segments with the same geometrical and material properties in laboratory tests during cable fabrication. The Q-statistics of the testing signals are plotted against the cable tension in Fig. 15. A parabolic regression curve was obtained as $y = -0.0006x^2 + 0.16x - 6.68$ with the R^2 value of 0.992, where x and y represent the tension and Q-statistics. Although this R^2 value is higher than that of the score-based method shown in Fig. 14(a), the estimating of cable tension becomes difficult above 110 kN. Additionally, the Q-statistics is a good measure of outliers such as tension changes from the reference value in the present cases. However, in contrast to the scores used in the proposed method, Q-statistic is apparently not sufficiently sensitive for quantifying the changes in tension.

4.5 Comparison with the notch frequency-based method

The performance of the proposed method was also compared with that of the notch frequency–based method. Fourier transform was performed on each received signal after zero padding at the end of the signal to enlarge the length of the signal to 400 for improving the frequency resolution. Examples of Fourier amplitude spectra for various tensions of 50, 70, 90, and 110 kN are shown in Fig. 16(a). It can be observed in each spectrum that a notch frequency band exists near the excitation frequency of 80 kHz and two frequency peaks (P_L and P_R) appear on two sides of 80 kHz. The main frequency component of the received signal without cable tension is around the excitation frequency (Sui *et al*. 2025), whereas it moved to 70 kHz (P_L) as the tension increased. The central frequency of P_R gradually increases with the cable tension, with the relationship between the central frequency of P_R and the tension as shown in Fig. 16(b). A linear regression curve was obtained as $y = 0.13x + 81.30$ with the R^2 value of 0.936, where x and y represent the tension and central frequency of P_R. The notch frequency–based cable tension estimation results are listed in Table 5, with the maximum error of 12.67%. Thus, the proposed PCA-based method demonstrates significantly better performance. Furthermore, it has been found that the amplitude of P_R keeps decreasing as the cable tension increases, which may be overlooked at larger cable tensions.

Table 5 Estimated cable tensions using notch frequency-based method

Real tensions (kN)	Average central frequencies of P_R (kHz)	Average estimated cable tensions (kN)	Average errors (%)
55	87.89	50.69	7.83
65	90.04	67.23	3.43
75	91.79	80.69	7.59
85	93.75	95.77	12.67
95	94.23	99.46	4.70
105	95.03	105.62	0.59
115	95.54	109.54	4.75
125	96.54	117.23	6.22

4.6 Additional discussion

The tension estimation accuracy of the proposed method

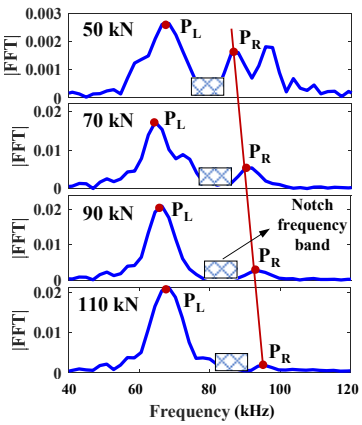

(a) Fourier amplitude spectra for different cable tensions

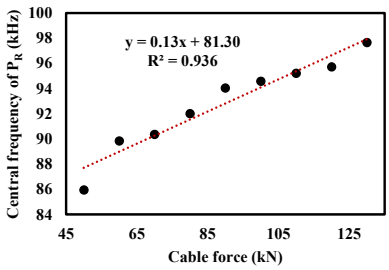

(b) Relationship between cable tensions and central frequency of P_R

Fig. 16 Notch frequency-based cable tension estimation results

is found to be better than those of the vibration–based and EM sensor–based methods, whereas it is equitant to that of the EME sensor–based method. Compared with the optic fiber method, the proposed method using MS transducers can be easily conducted without the need for pre-installation. During service life, local damages such as wire breakage and corrosion may occur on steel strands or cables. The amplitude of the received signal generally decreases when damage exists between the actuator and receiver. The current method is designed to detect cable tension in the undamaged region of the cable. Therefore, the damage state of the steel strand should be estimated at first. In our previous study, a roving MS transducer system was introduced to detect local damages on steel strands (Sui *et al*. 2025). It works particularly well for long steel cables. The roving MS transducer system is also suitable for estimating cable tension. By integrating these two techniques, local damages and cable tension can be detected simultaneously. The impact of environmental factors, such as temperature effects, on cable tension estimation accuracy has not been studied. The effects of these factors, along with the applicability of the method to cables with larger dimensions, different wire configurations, and damaged wires, need to be further investigated in future studies.

5. Conclusions

In this study, a PCA-based method was presented to estimate the cable tension of a seven-wire steel strand using the L(0, 1) guided waves. The dispersion properties of the steel strand under various cable tensions were analyzed using the SAFE method, and the wave velocity changes for each mode in the lower-frequency range were investigated. Experimental studies were carried out using a pair of MS transducers arranged in a pitch–catch configuration. Received signals at various cable tensions were extracted to construct the PCA model. Then, the score values most closely correlated with the tension variation were used to establish a regression curve with the applied cable tensions. Cable tensions were estimated for the test signals using the regression curve. The following conclusions can be drawn from this study:

(1) The wave velocity change of L(0, 1) mode due to variations in cable tension in a wide range of 50-130 kN was only 0.3% from SAFE analysis and 1.5% from real tests under the excitation frequency of 80 kHz, which indicates that it is difficult to detect the tension variations in practical.
(2) Cable tensions were accurately estimated using the score-based method. A linear regression curve was obtained between the scores and tensions. The maximum tension estimation error for the test cases was only 4.56%.
(3) The Q-statistic method performed well in the lower-tension range and is more convenient considering that the reference signal matrix is constructed by the signals from only a single tension level. However, its estimation accuracy deteriorated at tension levels above 110 kN.
(4) The maximum cable tension estimation error of the notch frequency–based method using the central frequency of P_R was 12.67%. Furthermore, the amplitude of P_R decreased with increasing cable tension, which may not be easily recognized at larger cable tensions.

Acknowledgments

This research was funded by the National Natural Science Foundation of China (Grant Nos. U24A20169, 51608478, 52361165658), Zhejiang Provincial Natural Science Foundation of China (Grant No. LGG21E080004), and Scientific Research Fund of Zhejiang Provincial Education Department (Grant No. Y202454348).

References

Bartoli, I., Castellazzi, G., Marzani, A. and Salamone, S. (2012), "Prediction of stress waves propagation in progressively loaded seven wire strands", In: *Conference on Sensors and Smart Structures Technologies for Civil*, *Mechanical*, *and Aerospace Systems*, San Diego, CA, USA, March.

Chaki, S. and Bourse, G. (2009), "Guided ultrasonic waves for non-destructive monitoring of the stress levels in prestressed steel strands", *Ultrasonics*, **49**(2), 162-171. https://doi.org/10.1016/j.ultras.2008.07.009

Chen, F. and Wilcox, P.D. (2007), "The effect of load on guided wave propagation", *Ultrasonics*, **47**(1-4), 111-122. https://doi.org/10.1016/j.ultras.2007.08.003

Chen, X., Zhu, J. and Lin, Y. (2022), "Attenuation characteristics of low frequency longitudinal guided waves generated by magnetostrictive transducers in bridge cables", *Mech. Syst. Signal Process*., **164**, p. 108296. https://doi.org/10.1016/j.ymssp.2021.108296

Cho, S., Jo, H., Jang, S., Park, J., Jung H.J., Yun, C.B., Spencer, B.F. and Seo, J.W. (2010), "Structural health monitoring of a cable-stayed bridge using wireless smart sensor technology: data analyses", *Smart Struct. Syst*., *Int. J*., **6**(5-6), 461-480. https://doi.org/10.12989/sss.2010.6.5_6.461

Duan, Y.F., Zhang, R., Dong, C.Z., Luo, Y.Z., Or, S.W., Zhao, Y. and Fan, K.Q. (2016), "Development of elasto-magneto-electric (EME) sensor for in-service cable force monitoring", *Int. J. Struct. Stabil. Dyn*., **16**(4), p. 1640016. https://doi.org/10.1142/s0219455416400162

Gravenkamp, H., Man, H., Song, C. and Prager, J. (2013), "The computation of dispersion relations for three-dimensional elastic waveguides using the scaled boundary finite element method", *J. Sound Vib*., **332**(15), 3756-3771. https://doi.org/10.1016/j.jsv.2013.02.007

Jana, D., Nagarajaiah, S., Yang, Y. and Li, S. (2022), "Real-time cable tension estimation from acceleration measurements using wireless sensors with packet data losses: analytics with compressive sensing and sparse component analysis", *J Civil Struct. Health Monitor*., **12**(4), 797-815. https://doi.org/10.1007/s13349-021-00526-4

Jo, H.C., Kim, S.H., Lee, J., Sohn, H.G. and Lim, Y.M. (2021), "Sag-based cable tension force evaluation of cable-stayed bridges using multiple digital images", *Measurement*, **186**, p. 110053. https://doi.org/10.1016/j.measurement.2021.110053

Kim, B.H., Jang, J.B., Lee, H.P. and Lee, D.H. (2010), "Effect of prestress force on longitudinal vibration of bonded tendons embedded in a nuclear containment", *Nuclear Eng. Des*.,

240(6), 1281-1289. https://doi.org/10.1016/j.nucengdes.2010.02.017

Kong, X., Liu, Z., Liu, H., Hu, J. and Deng, L. (2024), "Recent advances on inspection, monitoring, and assessment of bridge cables", *Automat. Constr.*, **168**, p. 105767. https://doi.org/10.1016/j.autcon.2024.105767

Kwun, H., Bartels, K.A. and Hanley, J.J. (1998), "Effects of tensile loading on the properties of elastic-wave propagation in a strand", *J. Acoust. Soc. Am.*, **103**(6), 3370-3375. https://doi.org/10.1121/1.423051

Liu, X., Wu, B., Qin, F., He, C. and Han, Q. (2017), "Observation of ultrasonic guided wave propagation behaviours in pre-stressed multi-wire structures", *Ultrasonics*, **73**, 196-205. https://doi.org/10.1016/j.ultras.2016.08.014

Mujica, L.E., Rodellar, J., Fernandez, A. and Guemes, A. (2011), "Q-statistic and T2-statistic PCA-based measures for damage assessment in structures", *Struct. Health Monitor. – Int. J.*, **10**(5), 539-553. https://doi.org/10.1177/1475921710388972

Ng, C.T., Yeung, C.R., Yin, T.Y. and Chen, L.J. (2022), "Stress evaluation of tubular structures using torsional guided wave mixing", *Smart Struct. Syst., Int. J.*, **30**(6), 639-648. https://doi.org/10.12989/sss.2022.30.6.639

Park, S., Lee, J.J., Yun, C.B. and Inman D.J. (2007), "Electro-mechanical impedance-based wireless structural health monitoring using PCA-data compression and k-mean clustering algorithms", *J. Intell. Mater. Syst. Struct.*, **19**(4), 509-520. https://doi.org/10.1177/1045389X07077400

Park, S., Kim, J. and Lee, C. (2022), "Residual tensile force estimation method for earth anchor using elasto-magnetic sensing system", *PlOS ONE*, **17**(3), p. e0264078. https://doi.org/10.1371/journal.pone.0264078

Piciucco, D., Foti, F., Geuzaine, M. and Denoel, V. (2024), "Bayesian forces identification in cable networks with small bending stiffness", *Struct. Health Monitor. – Int. J.*, **23**(4), 2135-2160. https://doi.org/10.1177/14759217231186957

Ren, L., Xiu, C., Li, H., Lu, Y., Wang, J. and Yao, X. (2018), "Development of elasto-magnetic (EM) sensor for monitoring cable tension using an innovative ratio measurement method", *Smart Mater. Struct.*, **27**(11), p. 115003. https://doi.org/10.1088/1361-665X/aae0b0

Rizzo, P. and Di Scalea, F.L. (2006), "Wavelet-based feature extraction for automatic defect classification in strands by ultrasonic structural monitoring", *Smart Struct. Syst., Int. J.*, **2**(3), 253-274. https://doi.org/10.12989/sss.2006.2.3.253

Sahota, J.K., Gupta, N. and Dhawan, D. (2020), "Fiber bragg grating sensors for monitoring of physical parameters: a comprehensive review", *Optical Eng.*, **59**(6), p. 060901. https://doi.org/10.1117/1.OE.59.6.060901

Schaal, C., Bischoff, S. and Gaul, L. (2013), "Analysis of wave propagation in periodic 3D waveguides", *Mech. Syst. Signal Process.*, **40**(2), 691-700. https://doi.org/10.1016/j.ymssp.2013.06.021

Shang, X.Q., Huang, T.L., Tang, L., Chen, H.P. and Ren, W.X. (2024), "Accurate and fast identification of time-varying tension in bridge cables via variational nonlinear chirp mode extraction", *Mech. Syst. Signal Process.*, **218**, p. 111574. https://doi.org/10.1016/j.ymssp.2024.111574

Sui, X.D., Zhang, R., Duan, Y.F., Luo, Y.Z. and Yun, C.B. (2025), "Detection of wire breakage in steel strands using a roving magnetostrictive guided wave detector and outlier analysis", *Smart Struct. Syst., Int. J.*, **35**(1), 53-64. https://doi.org/10.12989/sss.2025.35.1.053

Tang, Z.F., Sui, X.D., Duan, Y.F., Zhang, P.F. and Yun, C.B. (2021), "Guided wave-based cable damage detection using wave energy transmission and reflection", *Struct. Control Health Monitor.*, **28**(5), p. e2688. https://doi.org/10.1002/stc.2688

Treyssede, F. (2008), "Elastic waves in helical waveguides", *Wave Motion*, **45**(4), 457-470. https://doi.org/10.1016/j.wavemoti.2007.09.004

Tu, J.Q., Tang, Z.F., Yun, C.B., Wu, J.J. and Xu, X. (2021), "Guided wave-based damage assessment on welded steel I-beam under ambient temperature variations", *Struct. Control Health Monitor.*, **28**(4), p. e2696. https://doi.org/10.1002/stc.2696

Wang, G.D., Wang, M.L., Zhao, Y., Chen, Y. and Sun, B.N. (2006), "Application of magnetoelastic stress sensors in large steel cables", *Smart Struct. Syst., Int. J.*, **2**(2), 155-169. https://doi.org/10.12989/sss.2006.2.2.155

Wang, G., Lu, W., Yuan, C. and Kong, Q. (2022), "A cable tension identification technology using percussion sound", *Smart Struct. Syst., Int. J.*, **29**(3), 475-484. https://doi.org/10.12989/sss.2022.29.3.475

Wangchuk, S., Siringoringo, D.M. and Fujino, Y. (2022), "Modal analysis and tension estimation of stay cables using nonconatct vision-based motion magnification method", *Struct. Control Health Monitor.*, **29**(7), p. e2957. https://doi.org/10.1002/stc.2957

Xu, J., Li, Y. and Chen, G. (2019), "Effect of tensile force on magnetostrictive sensors for generating and receiving longitudinal mode guided waves in steel wires", *J. Sensors*, **2019**, p. 9512190. https://doi.org/10.1155/2019/9512190

Yao, Y., Yan, M. and Bao, Y. (2021), "Measurement of cable forces for automated monitoring of engineering structures using fiber optic sensors: A review", *Automat. Constr.*, **126**, p. 103687. https://doi.org/10.1016/j.autcon.2021.103687

Yim, J., Wang, M.L., Shin, S.W., Yun, C.B., Jung, H.J., Kim, J.T. and Eem, S.H. (2013), "Field application of elasto-magnetic stress sensors for monitoring of cable tension force in cable-stayed bridges", *Smart Struct. Syst., Int. J.*, **12**(3-4), 465-482. https://doi.org/10.12989/sss.2013.12.3_4.465

Zarbaf, S.E.H.A.M., Norouzi, M., Allemang, R.J., Hunt, V.J., Helmicki, A. and Venkatesh, C. (2018), "Ironton-Russell bridge: application of vibration-based cable tension estimation", *J. Struct. Eng.*, **144**(6), p. 04018066. https://doi.org/10.1061/(ASCE)ST.1943-541X.0002054

Zhang, P.F., Tang, Z.F., Duan, Y.F., Yun, C.B. and Lv, F.Z. (2018a), "Ultrasonic guided wave approach incorporating SAFE for detecting wire breakage in bridge cable", *Smart Struct. Syst., Int. J.*, **22**(4), 481-493. https://doi.org/10.12989/sss.2018.22.4.481

Zhang, R., Duan, Y.F., Zhao, Y. and He, X. (2018b), "Temperature compensation of elasto-magneto-electric (EME) sensors in cable force monitoring using BP neural network", *Sensors*, **18**(7), p. 2176. https://doi.org/10.3390/s18072176

Zhang, S.H., Zhang, H., Zhou, J.T., Liu, H.L., Ma, H. and Liao, L. (2022), "Alternating prestress monitoring of steel strands based on the magnetoelastic inductance method", *Measurement*, **194**, p. 111024. https://doi.org/10.1016/j.measurement.2022.11024

Zui, H., Shinke, T. and Namita, Y. (1996), "Practical formulas for estimation of cable tension by vibration method", *J. Struct. Eng.*, **122**(6), 651-656. https://doi.org/10.1061/(ASCE)0733-9445(1996)122:6(651)